AN INTEGRATED NUMERICAL PROCEDURE FOR FLUTTER AND FORCED RESPONSE ASSESSMENT OF TURBOMACHINERY BLADE-ROWS

F. Vanti – A. Agnolucci – L. Pinelli – A. Arnone

Department of Industrial Engineering
University of Florence
Via di S. Marta 3, 50139 Florence, Italy
Federico.Vanti@tgroup.de.unifi.it

ABSTRACT

Nowadays turbomachinery industry aims for more efficient and environmental friendly engines. Following this design trend, turbomachinery blades become lighter and more loaded, thus resulting prone to flutter induced vibrations. It is well known that vibrations can be also induced by aerodynamic forces due to rotor/stator interactions and, when Campbell crossings cannot be avoided, forced response analyses are also required to ensure a safe machine operation. This paper presents an integrated procedure to investigate flutter and forced response and its application to a 1 and 1/2 low pressure transonic compressor stage. The method is based on the open-source FEM solver (CalculiX) and on the in-house CFD code (TRAF). Moreover, a dedicated tool-chain, able to automatically exchange boundary conditions between the two solvers was implemented. For flutter assessment of the rotor, frequencies and mode-shapes are computed with the FEM code and imposed to the CFD flutter analyses (URANS computations with moving blades). At the same time, an unsteady CFD analysis is carried out to evaluate the aerodynamic excitations on the rotor due to up/downstream stators. The different pressure harmonics on the rotor surface, extracted by a run-time DFT algorithm, are used as external loads for forced response analyses. The aerodynamic damping obtained by flutter computations is also included in these dynamic analyses. Finally, the numerical results are compared with experimental data acquired in the context of the EU FUTURE project. Such comparisons confirm the applicability of the above-mentioned procedure in the blade-row design loop.

NOMENCLATURE

E	Young's Module
R	Rotation Matrix
t	Translation Vector

Greek:

ν	Poisson's Ratio
ω	Angular Frequency
ρ	Density
ξ	Critical Damping Ratio

Subscripts:

$_s$	Static Quantity
$_t$	Total Quantity

Acronyms:

BCs	Boundary Conditions
CFD	Computational Fluid Dynamics
CSD	Computational Solid Dynamics
FEM	Finite Element Method
DFT	Discrete Fourier Transform
EO	Engine Order
FRF	Frequency Response Function
FS	Fatigue Stress
PR_{tt}	Pressure Ratio
UTS	Ultimate Tensile Strength
$VIGV$	Variable Inlet Guide Vane

INTRODUCTION

The greening of aviation industry requires the design of more efficient and quieter engines. As a result engine components become lighter and slender, and at the same time, subjected to higher aerodynamic loads. An accurate aeromechanical characterization of engine bladerows is thus necessary during the design phase to avoid or control vibrations issues related to flutter and forced response phenomena which can even lead to high cycle fatigue failures. The forced response phenomenon is strictly connected to the unsteadiness of multi-stage turbomachineries. Flow distortions, mainly due to wakes and potential effects, generate periodic multi-row excitations for blade rows and may cause excessive vibration amplitudes and alternate stresses when the excitation frequency interferes with the natural frequency of the blade. Usually, the highest forced response occurs at frequencies synchronous with the rotating frequency (Engine Order EO). On the other hand, flutter is an unstable aeroelastic phenomenon and its onset is due to a negative damping caused by blade-flow interaction. In case the damping of the mechanical system is relatively small and cannot equalize the negative damping coming from the flow, the vibration amplitude may increase indefinitely or reach a limit cycle amplitude leading to potential blade row damage. Flutter occurrences usually happen at high flow velocities and at low blade natural frequencies, asynchronous with the rotating frequency. Flutter and forced response phenomena can be thus considered as one the main cause of high cycle fatigue failure of turbomachinery blades and are well known in the literature (Kielb and Chiang (1992), Srinivasan (1997)). For this reason, a number of numerical methods have been developed to achieve safe bladerow design (Moffatt and He (2003), Ning et al. (2003), Eichner and Belz (2018)). All these methods are based on structural dynamic solvers to evaluate, for example, components mode-shapes and on aerodynamic codes to compute the fluid flow unsteady response caused by rotor/stator interactions or by vibrating profiles. Usually CFD solvers implement different methodologies with different level of complexity (e.g. linear, time-linearized, harmonic balance or non-linear methods) (Poli et al. (2015), Frey et al. (2015)). Therefore aeromechanical verification involve structural and aerodynamic analyses which have to exchange boundary conditions in an uncoupled or coupled approach. For instance, flutter analyses require the blade mode shapes coming from modal computation, while forced response verifications need aerodynamic unsteady loading computed by unsteady CFD simulations. Nowadays, all structural and aerodynamic numerical tools are mature and validated and are applied to evaluate the effect of random and intentional mistuning (Beirow et al. (2019), Figaschewsky et al. (2017), Vanti et al. (2017), Biagiotti et al. (2018)), the impact of a multi-rows environment (Mao et al. (2018), Barreca et al. (2018)) and also the interaction between flutter and forced response phenomena (Mao and Kielb (2017)). Therefore it becomes more and more important to increase code integration to implement stand-alone procedures able to assess both flutter and forced response phenomena in a same framework. In this context, the paper presents the integration of the FEM open-source CalculiX solver with the URANS TRAF code developed at the University of Florence for the aeromechanical design of turbomachinery bladerows.

NUMERICAL STRATEGY AND COMPUTATIONAL SETUP

The numerical procedure, developed during this activity, aims to reduce the design process time related to the aeroelastic analyses. This procedure consists in transferring results obtained from FEM results to CFD and vice-versa. The work-flow (reported in Fig. 1) shows an overview of the overall numerical strategy: both solid and fluid analyses are carried on. The pre-postprocessing tool has been developed in Python language to handle all the boundary con-

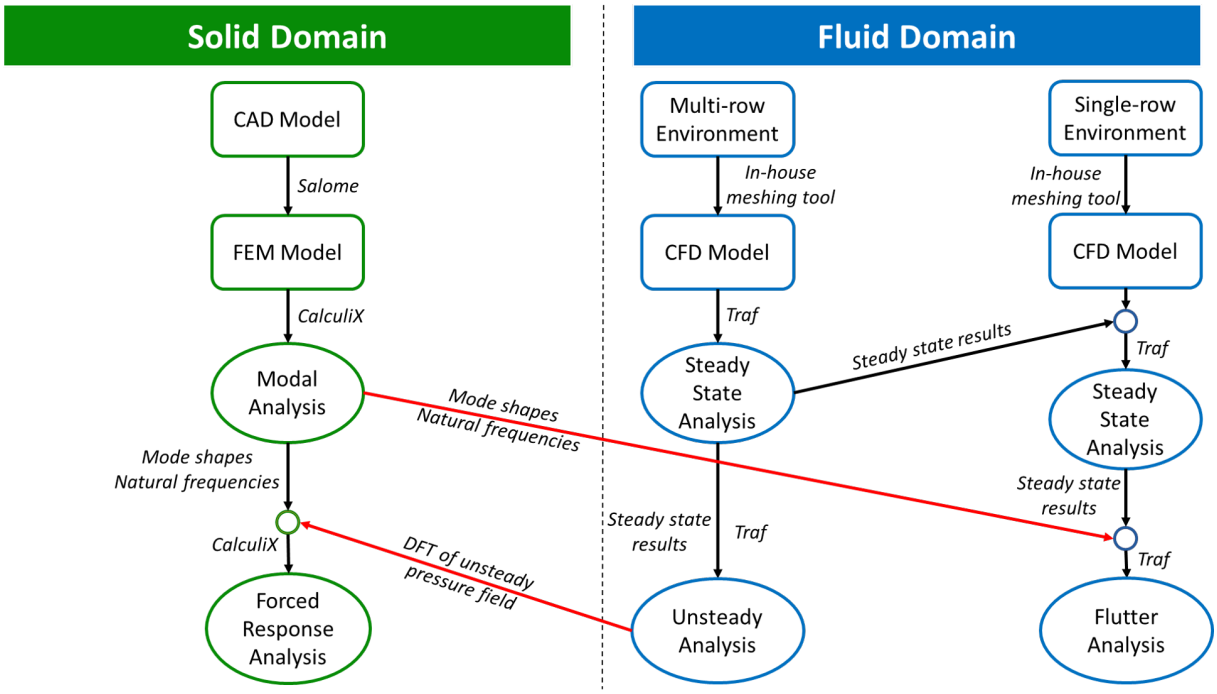

Figure 1: **Work-flow chart**

ditions exchange on blade surface from solid to fluid and vice-versa and to automatically apply a roto-translation between CSD and CFD domain, if needed. These aspects drastically reduce the time for the simulation setup and guide the user step by step, lowering the risk of possible mistakes. Below, the description of all the steps of procedure connected by the pre-postprocessing tool.

Aerodynamic setup

Before starting with any aeroelastic simulations, a steady state aerodynamic analysis is required. This analysis is necessary to verify the operating condition of the row under investigation and also to extract steady state load for the accurate modal analysis computation. Such numerical evaluation must be performed on the operational blade configuration, the so called "hot geometry". Steady state field results are also used as initialization for all the following unsteady simulations.

Hot geometry evaluation

The evaluation of the hot geometry consists in performing a steady stress analysis taking into account the effects of the rotational speed of the rotor onto the cold geometry. The effect of centrifugal force tends to deswirl the blade changing the blade stagger at different spanwise positions. This analysis can be easily handled by using CalculiX to perform a static deformation analysis. Then, the developed pre-postprocessing tool is used to automatically apply blade deformation on the original geometry and to obtain the hot blade surfaces. This geometry will be used for the CFD discretization of the compressor rotor.

Multi-row mesh generation

Since one of the main aim of this activity is to analyze the rotor excitation due to upstream wakes and downstream potential field, a multi-row domain must be taken into account. The overall domain is composed by a VIGV, a rotor and a stator consisting of 15, 21 and 29 blades, respectively. Structured grids are generated by an in-house meshing tool starting from the airfoil sections at different span-wise positions and from the endwall surfaces definitions within the meridional channel. Different grid topologies are used for the entire domain discretization: O-type grids are built around the blade surface, while H-type grids are included in the inter-row gaps. The O-type grids are chosen in order to have a better resolution of the boundary layer region over the blade surface and the grid stretch orthogonal to the surface is chosen to ensure a y_+ lower than 1. H-type grids are used for the uniform discretization of the inter-rows channel. The meridional visualization of the 1 and 1/2 compressor stage is shown in the left of Fig. 2. The domain under investigations is bound inside the two red lines shown in the sketch. The overall 3D mesh size is around 7 M of cells and a mesh re-clustering is applied near the endwall regions as can be noticed on the 3D mesh visualization on the right of Fig. 2.

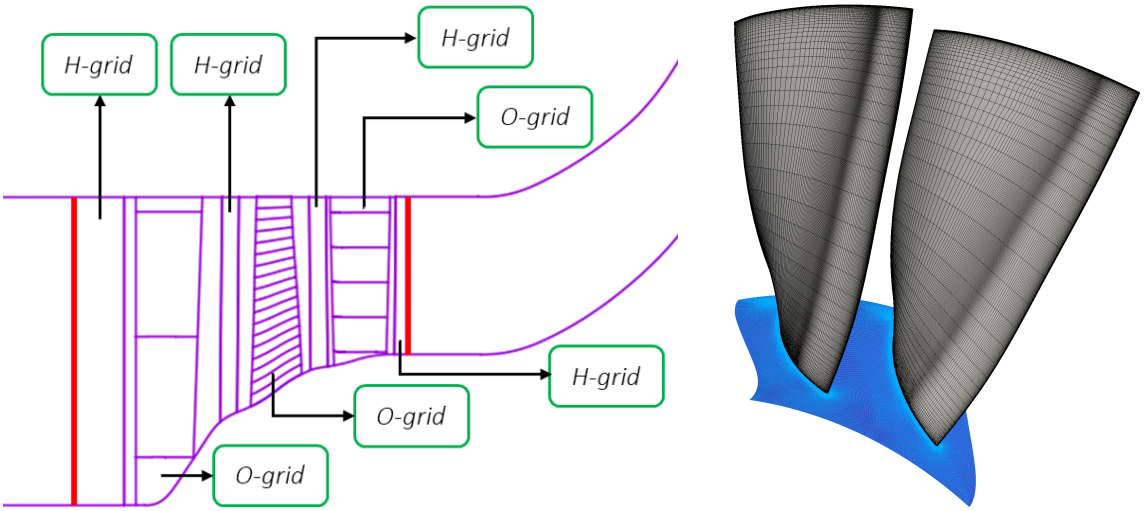

Figure 2: **Fluid domain: meridional sketch (left) and 3D rotor blade grid (right)**

Multi-row steady state analysis

After the domain discretization, a multi-row steady state analysis is performed by using the TRAF code. TRAF code is a 3D RANS/URANS aerodynamic solver, developed at the University of Florence (Arnone (1994), Arnone et al. (1993)). A single vane per row is computed for the CFD steady state analysis, leading to a consistent cost saving of the computational time. The following table summarizes the main quantities for the operating point under investigation:

Mass Flow [kg/s]	Inlet p_t [Pa]	Outlet p_s [Pa]	PR_{tt} [-]	Rotational Velocity [rpm]
12.39	101325	120540	1.18	16000

Radial profiles of total pressure and temperature, blade to blade and meridional angles, measured in the context of the FUTURE project, are imposed at the inlet section of the domain,

while static pressure is imposed downstream with a radial equilibrium distribution. For this operating point, the VIGV stagger angle is equal $0°$ and the flow (air) is modeled as an ideal gas. The numerical setup employs a $k-\omega$ turbulence model and a mixing plane approach.

Flutter analysis

Solid grid mesh generation

This tool-chain step consists in generating a tetrahedral mesh for the blade sector using the open-source Salome suite. The solid domain is composed of a single-pitch bladerow sector including blade and disk (blisk). The number of elements was chosen to achieve accurate results while maintaining a low computational cost: a mesh of 40000 quadratic tetrahedron elements was generated for all the FEM analyses.

Titanium Ti-6Al-4V	
E	116.5 [GPa]
ν	$3.225 \cdot 10^{-1}$ [-]
ρ	$4.43 \cdot 10^{+3}$ [$\frac{kg}{m^3}$]
UTS	900 [MPa]
FS	450 [MPa]

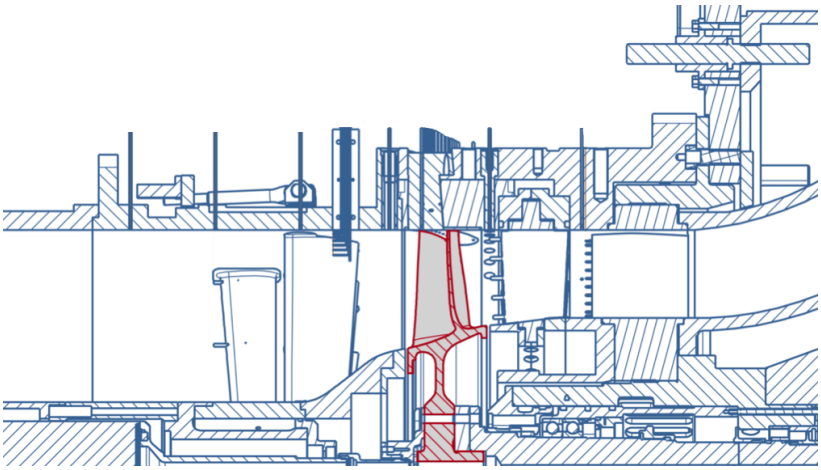

Figure 3: **Material properties (left) and test-rig meridional sketch (right)**

Modal analysis

The modal analysis is performed by using the open-source FEM solver CalculiX (Dhondt (2004)). The blisk is made of titanium Ti-6Al-4V and its mechanical properties are listed in the table included in Fig. 3. Although the rotor (highlighted in red in the sketch on the right side of Fig. 3) consists in 21 blades, only one single-pitch sector is considered by exploiting cyclic symmetry boundary conditions in order to reduce the computational cost. Axial, radial and tangential constraints due to blisk connection with the shaft are imposed both for static and modal analysis and centrifugal forces due to the rotational speed (16000 rpm) are also taken into account. It is worth noticing that the results, in terms of eigenfrequencies and mode shapes, coming from a modal analysis have a strong impact on the future steps of the analysis.

Mode shape transfer and mesh deformation strategy

To perform flutter analyses, the computational fluid domain has to be deformed according to row oscillation. A mode shape transfer technique is used to interpolate a real or complex mode shape, coming from the modal analysis, to the blade surface within the CFD mesh (Pinelli et al. (2009)). The internal grid deformation is built by using an algebraic method distributing the largest deformations where the biggest mesh elements are, while maintaining low deformations of the smallest elements to avoid cells intertwining. Since in general, the FEM and CFD models

have not the same frame of reference, a tool performing an automatic roto-translation of the CSD mesh onto the CFD grid has been developed. By defining two set of nodes within CSD and CFD meshes, in corresponding positions (e.g. LE and TE at the tip and LE at the hub of both solid and fluid grid), the rotation matrix R and translation vector t are computed by means of an optimization procedure that minimizes the residual (Sorkine-Hornung and Rabinovich (2017)), defined as follows:

$$\sum_{i=1}^{N} w_i \mid\mid (Rp_i + t) - q_i \mid\mid \tag{1}$$

where N is the number of CSD and CFD nodes chosen for the optimization (usually 3 nodes are enough to obtain the method convergence), w_i are the weights used for the minimization, p_i and q_i are the coordinates vectors of the i-th node of CSD and CFD domain, respectively.

Single row flutter computation

As already shown in Fig. 1, steady state and mode shapes results, already computed, are used as input data for the uncoupled flutter analysis. Flutter assessment is only focused on the rotor row where the risk of flutter occurrence is significantly higher. During the simulation, each period of blade oscillation is discretized into equally-spaced time instants in which the computational domain is rebuilt by the aeroelastic solver, computing the unsteady pressure response due to the blade vibration. When the solution is converged and periodic, flutter stability is assessed by checking the sign of the aerodynamic work done by the fluid onto the blade during one vibration period (energy method (Carta (1967))). A phase lagged approach is applied on the circumferential periodic boundaries of the single angular pitch domain to solve all the possible traveling waves. Two vanes of the rotor are simulated in order to speed-up the convergence and reduce the CPUs time requirement. (Giovannini et al. (2014)).

Forced response analysis

Multi-row unsteady analysis

A further step of the procedure work-flow consists in performing a multi-row unsteady analysis. Since the blade counts does not allow a reduction of the computational domain to an angular section, a full annulus approach has to be used. This means that the entire wheel must be simulated leading to an higher computational cost. Usually to reach the flow periodicity, 4 rotor revolution periods are necessary. The solution obtained by the steady state analysis are used as flow initialization. Time resolution was chosen in order to accurately solve the first 3 harmonics of the highest blade passing frequency related to the stator potential field disturbance. Following this rule, 725 physical time steps are used for a whole rotor revolution and each physical time step is converged with up to 15 sub-iterations. When the solution periodicity is obtained, a run-time DFT can be activated to extract the desired pressure harmonics in the entire domain. Finally, the pre-postprocessing tool is also used to extract the pressure harmonics on the blade surfaces in a suitable format for CalculiX.

Forced response computation

Forced response analysis is the final step of the presented procedure. The strongest aerodynamic sources of excitation for the rotor row are the upstream wakes and downstream potential effects. The external forcing functions in terms of unsteady pressure distribution (real and

imaginary part over the blade surface) coming from the unsteady analysis are transferred by the pre-postprocessing tool from the CFD grid nodes to the CSD surface elements: the main EOs under investigation are 15, 29, 30 and 58 (related to the first and second harmonic of the upstream-downstream sources of excitation). The FEM analysis is carried out by keeping the same constraints and pre-stressed conditions imposed for the previous modal analyses. The aerodynamic damping obtained from the uncoupled flutter analysis is also included within dynamic simulation.

RESULTS

Modal analysis results

The modal analysis results are presented for the first 3 mode families, the most critical for flutter stability. All the results are summarized in Fig. 4 in terms of eigenvalues and eigenmodes.

ND	F1 [Hz]	F2 [Hz]	F3 [Hz]
0	559.7	1420.8	1539.9
1	553.4	1092.1	1449.5
2	552.5	1107.4	1464.6
3	562.6	1439.9	1788.2
4	564.3	1446.6	1808.9
5	565.2	1450.5	1813.1
6	565.9	1453.6	1815.0
7	566.4	1455.7	1816.0
8	566.7	1457.2	1816.6
9	566.8	1458.0	1817.0
10	566.9	1458.4	1817.2

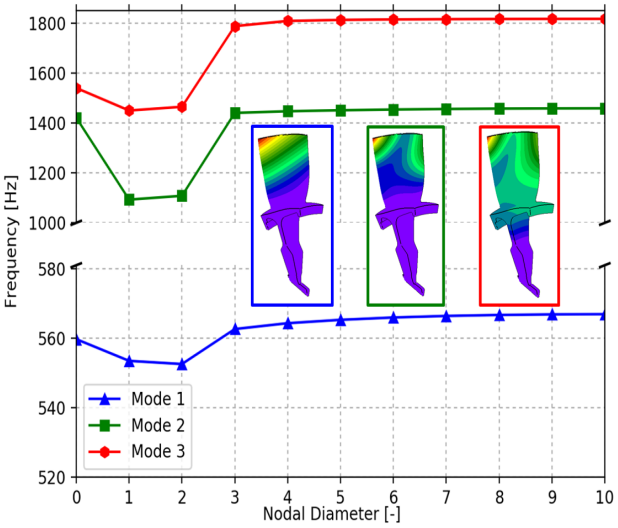

Figure 4: **Table (left) and plot (right) of blisk frequencies**

The blisk configuration setup with cyclic symmetry conditions ensures more accurate results than the blade alone analysis. Looking at the frequency curves for the three families, a saturated trend for the highest nodal diameters can be observed. This trend can be explained by considering the disk participation on the overall mode shape. For low nodal diameters, the blades oscillate almost in phase and the disk takes part in the overall deformation thus lowering the vibration frequencies. On the other hand, for high nodal diameters, the disk does not participate to the deformation and the frequencies tends to remain constant.

Aerodynamic results

The main aerodynamic data are extracted from the steady state computations. Spanwise distributions of circumferentially-average flow quantities are acquired during the experimental campaign and are used both to impose the CFD boundary conditions and to check the solution accuracy. At the 1 and 1/2 stage inlet, the radial profile distributions of total pressure and temperature and flow angle are imposed. On the other hand, only the static pressure distribution is imposed at the domain outlet. The comparison with experimental data are focused on the inlet and outlet of the rotor as the aeromechanical investigation is dedicated to this component.

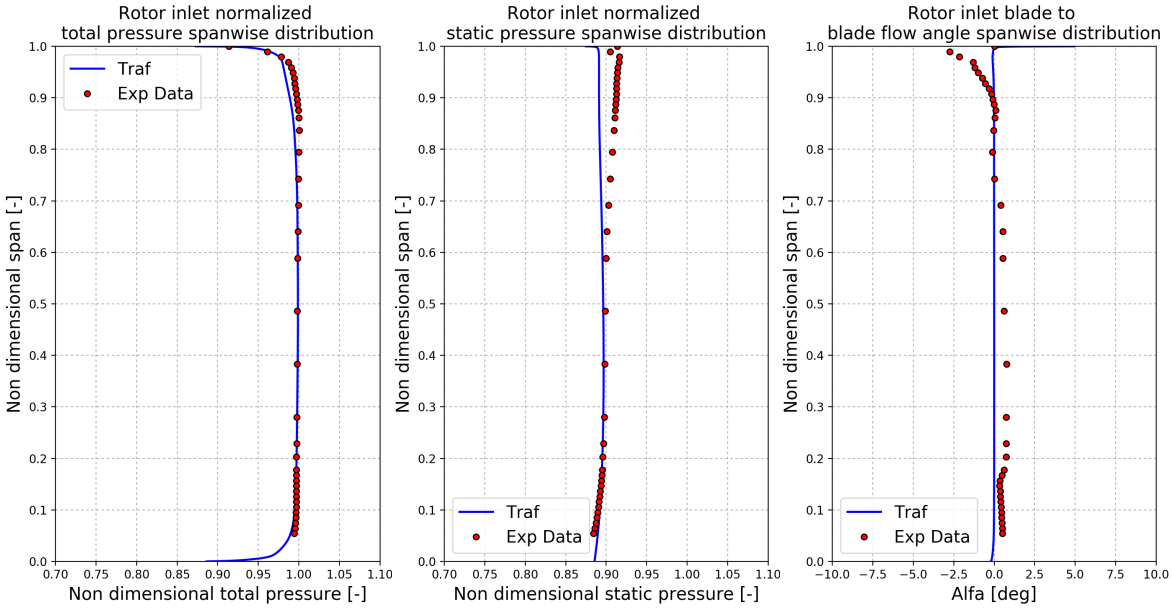

(a) Total pressure (b) Static pressure (c) Blade to blade flow angle

Figure 5: **Rotor inlet non-dimensional spanwise distributions**

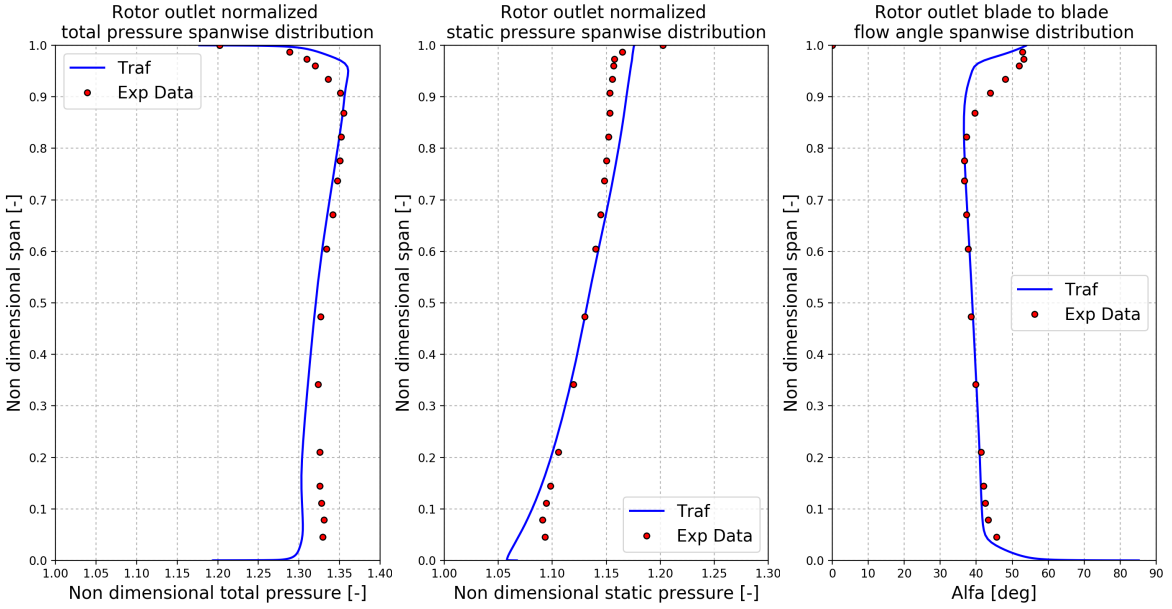

(a) Total pressure (b) Static pressure (c) Blade to blade flow angle

Figure 6: **Rotor outlet non-dimensional spanwise distributions**

Looking at this comparisons in terms of total and static pressure and blade to blade angle, it can be observed a fairly good agreement (Fig. 5 and Fig. 6). The main discrepancies are located in the tip region of the rotor outlet. This can be due to the simplified clearance model used for the rotor and VIGV (Cozzi et al. (2017)), which is not completely able to capture the tip vortex evolution. Anyway, this aspect does not have a strong impact on the rotor aeromechanic as the discrepancies are located in a narrow area. As the operating point is transonic, the major non-linear effects are due to the shock impingement on the blade surface, which strongly influences the flutter stability.

Flutter results

Different unsteady simulations with vibrating row (one for each possible IBPA) have been performed to assess the rotor stability. Each computation with phase-lagged conditions lasted 10 oscillation periods to reach the flow periodicity. A single oscillation is discretized in time with 80 equally-spaced instants. Each physical time step is solved with up to 20 subiterations of the dual time-stepping method to achieve a flat residual curve in each time step. The flutter solution in terms of unsteady pressure on the oscillation blade is used to evaluate the aerodynamic work and, in turn, the critical damping ratio. The sign of these quantities can be employed to assess flutter stability. Looking at the critical damping ratio, a positive sign indicates a stable condition in which the row dissipates energy to the fluid, whereas a negative value denotes an unstable condition in which the energy goes from the fluid to the blade, enhancing the vibration. The amplitude growth depends on the magnitude of the aerodynamic work and sometimes the amplitude may stabilize in a limit cycle configuration. The flutter analyses have been performed

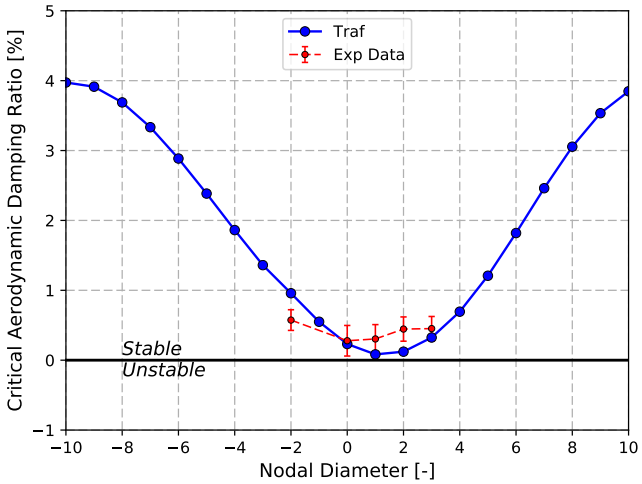

Figure 7: **Critical damping ratio vs. nodal diameter for the first bending family**

for all the possible nodal diameters, although the experimental values are only available for few nodal diameters as presented in (Barreca et al. (2018)). Each experimental value has its uncertainly reported with an error bar as shown Fig. 7. As expected, the numerical curve shows a sinusoidal trend with high damping values for higher IBPAs. The experimental curve for low nodal diameter is more flat, yet the experimental data are well captured by numerical flutter simulations.

Forced response results

Unsteady computations provide the harmonic of pressure response caused by rotor-stator interactions. Fig. 8 shows the distributions of the amplitude and phase for the main pressure harmonics acting on the blade surface. Comparing the amplitude distributions, it is clearly visible how the VIGV wakes have a great impact on the rotor rather than the stator potential effect, despite of the wide gap between the VIGV and the rotor. These pressure fields represent the unsteady excitations acting on the rotor at the different frequencies and are extracted by means the pre-postprocessing tool from the unsteady solution and imposed to the blade surface after the required roto-translation for the following dynamic simulation.

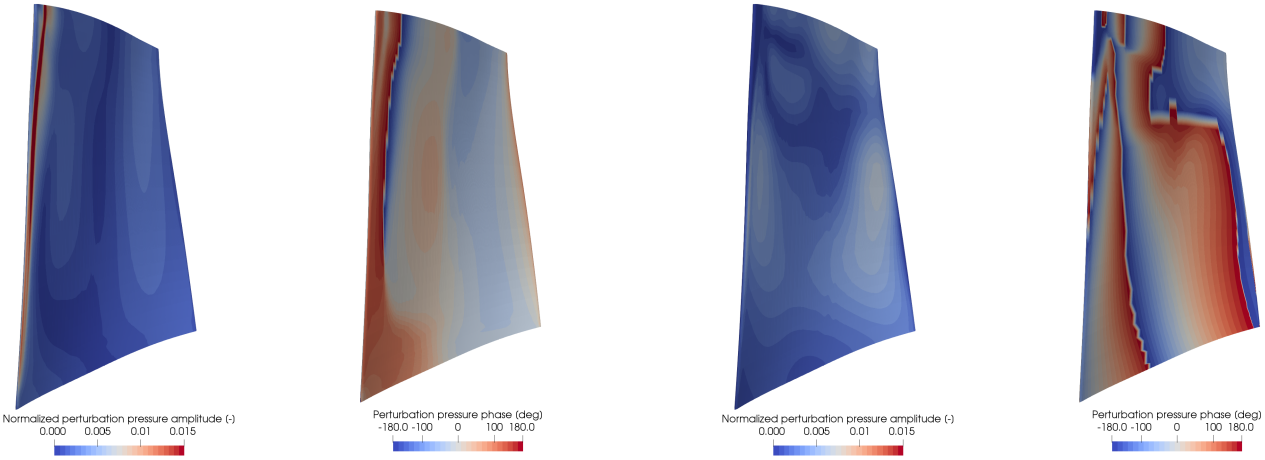

(a) EO 15 - VIGV (b) EO 29 - Stator

Figure 8: **Amplitude and phase of unsteady pressure harmonics**

Before computing the forced response, it is worth noticing that in the Campbell diagram of the rotor (see Fig. 9) there are no crossings between blisk eigenfrequencies and the engine order related to the downstream/upstream row disturbances (EO15 and EO29) at 16000 rpm (red vertical line in Fig. 9). This is due to the fact that the rotor was designed to avoid Campbell crossings at the operating point where aerodynamic damping is measured. Fig. 10 shows the FRF curves, obtained using CalculiX solver, for the point at the blade tip which experiences the maximum displacement. These results are related to the EO15 and EO29 excitation due to VIGV wakes and stator potential field. It has to be noticed that displacements caused by EO15 are one order of magnitude greater than the ones due to EO29. Resonance frequencies can be easily appreciated in the plots and low displacements are computed for the EO15 (4000 Hz)

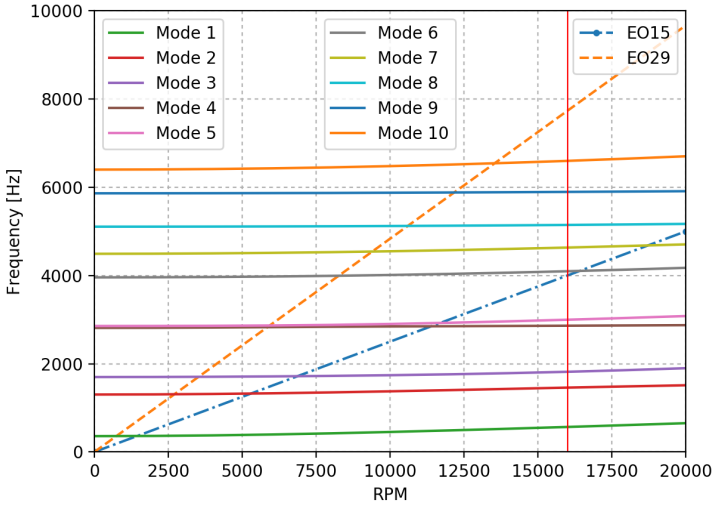

Figure 9: **Campbell Diagram**

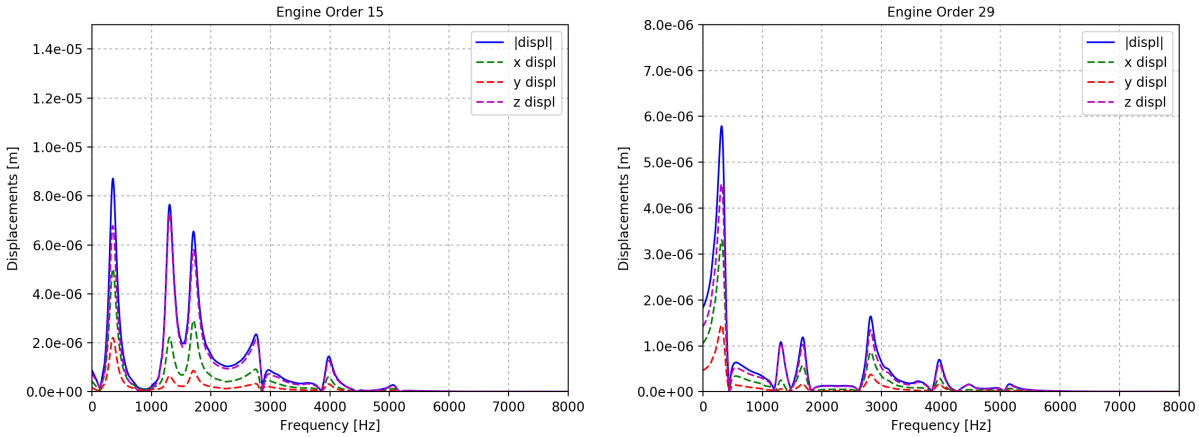

(a) EO 15 - VIGV

(b) EO 29 - Stator

Figure 10: **FRF results**

and EO29 (7733 Hz). As can be seen, the amplitude results related to the frequencies under investigation are very low. Nevertheless, a HCF evaluation, which confirms the infinite life of the rotor blisk, has been carried out using the Goodman diagram to check the overall procedure.

CONCLUSIONS

Aeromechanical characterization of turbomachinery components is becoming more and more important during design phase as the bladerows are now slender and more loaded. Flutter and forced response vibrations have to be considered as they may lead to high cycle fatigue failures. To face all these aspects from a numerical point of view, two main type of analyses are required: FEM and CFD computations which have to exchange boundary conditions on the blade surfaces. Classical CFD flutter simulations need for mode shapes coming from modal analyses, whereas forced response assessments require blade unsteady loads from unsteady simulations. Frequently, FEM and CFD models do not have the same frame of reference and need to be scaled to make blade surfaces coincident for data transfer with different interpolation methods. FEM and CFD methods included in this numerical procedure are mature and validated, so it is important to integrate the solvers within a numerical procedure to reduce setup time and to avoid user mistakes. To do this, a pre-postprocessing tool has been developed to handle the boundary conditions transfer between FEM and CFD domains. The tool ensures an integration of the different numerical simulations and has been applied for flutter and forced response assessment of a rotor blisk within a 1 and 1/2 stage compressor rig, consisting of VIGV, rotor and stator. All the numerical analyses have been described in detail and the BCs transfers, performed by the pre-postprocessing tool, are highlighted. Flutter and forced response results show a good agreement with experimental values acquired during the FUTURE project. As far the flutter assessment is concerned, the rotor shows an overall stability for the operating condition under investigation. At this operating point, no Campbell crossings are present for the EO of major concern (EO15 and EO29), yet the forced response procedure has been applied to check its correct working. All the results confirm the correct integration of FEM open-source CalculiX with URANS TRAF code for flutter and forced response analyses.

ACKNOWLEDGEMENTS

The authors wish to acknowledge the European Commission of FUTURE project for the permission to publish.

REFERENCES

Arnone, A. (1994). Viscous analysis of three-dimensional rotor flow using a multigrid method. *Journal of Turbomachinery*, 116:435–445.

Arnone, A., Liou, M.-S., and Povinelli, L. (1993). Multigrid calculation of three-dimensional viscous cascade flows. *Journal of Propulsion and Power*, 9(4):605–614.

Barreca, P. Pinelli, L., Vanti, F., and Arnone, A. (2018). Aeroelastic investigation of a transonic compressor rotor with multi-row effects. In *73rd Conference of the Italian Thermal Machines Engineering Association (ATI 2018)*. Associazione Termotecnica Italiana.

Beirow, B., Kühhorn, A., Figaschewsky, F., Bornhorn, A., and Repetckii, O. V. (2019). Forced response reduction of a blisk by means of intentional mistuning. *Journal of Engineering for Gas Turbines and Power*, 141(1):011008.

Biagiotti, S. Pinelli, L., Poli, F., Vanti, F., and Arnone, A. (2018). Numerical study of flutter stabilization in low pressure turbine rotor with intentional mistuning. In *73rd Conference of the Italian Thermal Machines Engineering Association (ATI 2018)*. Associazione Termotecnica Italiana.

Carta, F. O. (1967). Coupled blade-disk-shroud flutter instabilities in turbojet engine rotors. *Journal of Engineering for Power*, 89(3):419–426.

Cozzi, L., Rubechini, F., Marconcini, M., Arnone, A., Astrua, P., Schneider, A., and Silingardi, A. (2017). Facing the challenges in cfd modelling of multistage axial compressors. In *ASME Turbo Expo 2017: Turbomachinery Technical Conference and Exposition*. American Society of Mechanical Engineers. ASME paper GT2017-63240.

Dhondt, G. (2004). The finite element method for three-dimensional thermomechanical applications. *Statistical Tools for Simulation Practitioners*. Wiley, New York.

Eichner, F. and Belz, J. (2018). Application of the modal approach for prediction of forced response amplitudes for fan blades. In *ASME Turbo Expo 2018*. ASME paper GT2018-75239.

Figaschewsky, F., Kühhorn, A., Beirow, B., Nipkau, J., Giersch, T., and Power, B. (2017). Design and analysis of an intentional mistuning experiment reducing flutter susceptibility and minimizing forced response of a jet engine fan. In *ASME Turbo Expo 2017*. ASME paper GT2017-64621.

Frey, C., Ashcroft, G., and Kersken, H.-P. (2015). Simulations of unsteady blade row interactions using linear and non-linear frequency domain methods. In *IGTI ASME Turbo Expo*. ASME paper GT2015-43453.

Giovannini, M., Marconcini, M., Arnone, A., and Bertini, F. (2014). Evaluation of unsteady computational fluid dynamics models applied to the analysis of a transonic high-pressure turbine stage. *Proceedings of the Institution of Mechanical Engineers, Part A: Journal of Power and Energy*, 228(7):813–824.

Kielb, R. and Chiang, H.-W. (1992). Recent advancements in turbomachinery forced response analyses. In *30th Aerospace Sciences Meeting and Exhibit*, page 12.

Mao, Z., Hegde, S., Pan, T., Kielb, R. E., Zori, L., and Campregher, R. (2018). Influence of rotor-stator interaction and reflecting boundary conditions on compressor forced response. In *ASME Turbo Expo 2018*. ASME paper GT2018-75232.

Mao, Z. and Kielb, R. E. (2017). Interaction of concurrent forced response and flutter phenomena in a compressor stage. In *ASME Turbo Expo 2017*. ASME paper GT2017-63376.

Moffatt, S. and He, L. (2003). Blade forced response prediction for industrial gas turbines.part 1: methodologies. In *ASME Turbo Expo 2003*, pages 407–414. ASME paper GT2003-38640.

Ning, W., Moffatt, S., Li, Y., and Wells, R. G. (2003). Blade forced response prediction for industrial gas turbines. part 2: verification and application. In *ASME Turbo Expo 2003*, pages 415–422. ASME paper GT2003-38642.

Pinelli, L., Poli, F., Arnone, A., and Schipani, C. (2009). A time-accurate 3D method for turbomachinery blade flutter analysis. In 12^{th} *International Symposium on Unsteady Aerodynamics, Aeroacoustics and Aeroelasticity of Turbomachines (ISUAAAT)*. September 1–4, London, UK, paper I12-S8-3.

Poli, F., Pinelli, L., and Arnone, A. (2015). Aeroelastic stability analysis of a non-rotating annular turbine test rig: a comparison between a linearized and a non-linear computational method. In *22nd International Congress on Sound and Vibration*.

Sorkine-Hornung, O. and Rabinovich, M. (2017). Least-squares rigid motion using svd. *no*, 3:1–5.

Srinivasan, A. (1997). Flutter and resonant vibration characteristics of engine blades. *Journal of engineering for gas turbines and power*, 119(4):742–775.

Vanti, F., Pinelli, L., Poli, F., and Arnone, A. (2017). Aeroelastic investigation of turbine blade assemblies: Cluster system and mistuned rows. In *European Conference on Turbomachinery Fluid dynamics and Thermodynamics*, pages 3–7.